Grounding and Calving Cycle of Mertz Ice Tongue Revealed by Shallow Mertz Bank

Xianwei Wang[1,2], David M. Holland[2,3], Xiao Cheng[1,5] and Peng Gong[4,5]

1. State Key Laboratory of Remote Sensing Science, and College of Global Change and Earth System Science, Beijing Normal University. Beijing 100875, China.

2. Center for Global Sea Level Change, New York University Abu Dhabi. Abu Dhabi, United Arab Emirates.

3. Courant Institute of Mathematical Sciences, New York University. New York 10012, United States of America.

4. Ministry of Education Key Laboratory for Earth System Modeling, and Center for Earth System Science, Tsinghua University, Beijing, China 100084.

5. Joint Centre for Global Change Studies, Beijing, China.

Correspondence to: *wangxianwei0304@163.com*

Abstract

A recent study, using remote sensing, provided evidence that a seafloor shoal influenced the 2010 calving event of the Mertz Ice Tongue (MIT), by partially grounding the MIT several years earlier. In this paper, we start by proposing a method to calculate Firn Air Content (FAC) around Mertz from seafloor-touching icebergs. Our calculations indicate the FAC around Mertz region as 4.87±1.31 m. We then design an indirect method of using freeboard and sea surface height data extracted from ICESat/GLAS, FAC, and relatively accurate seafloor topography to detect grounding sections of the MIT between 2002 and 2008 and analyze the process of grounding prior to the calving event. By synthesizing remote sensing data, we point out that the grounding position was localized northeast of the Mertz ice front close to the Mertz Bank. The grounding outlines of the tongue caused by the Mertz Bank are extracted as well. From 2002 to 2008, the grounding area increased and the grounding became more pronounced. Additionally, the ice tongue could not effectively climb over the Mertz Bank in following the upstream ice flow direction and that is why MIT rotated clockwise after late 2002. Furthermore, we demonstrate that the area-increasing trend of the MIT changed little after calving (~36 km^2/a), thus allowing us to use remote sensing to estimate the elapsed time until the MIT can reground on and be bent by the shoal. This period is approximately 70 years. Our observations suggest that the calving of the MIT is a cyclical process controlled by the presence of the shallow Mertz Bank location and the flow rate of the tongue. This calving cycle also explains the cyclic variations in sea-surface conditions around the Mertz detected by earlier studies.

Keywords: Mertz Ice Tongue, firn air content, grounding, Mertz Bank, calving cycle.

1. Introduction

Surface-warming induced calving or disintegration of floating ice has occurred in Antarctica, such as the Larsen B ice shelf (Scambos et al., 2000, 2003; Domack et al., 2005; Shepherd et al., 2003). While surface or sub-surface melting has largely been recognized to contribute to floating ice loss in Antarctica (Depoorter et al., 2013), calving caused by interaction with the seafloor has not been widely considered. The Mertz Ice Tongue (MIT) was reported to have calved in 2010, subsequent to being rammed by a large iceberg, B-9B (Legresy et al. 2010). After the calving, the areal coverage of Mertz polynya, sea ice production and dense, shelf water formation in the region changed (Kusahara et al. 2011; Tamura et al. 2012). However, the iceberg collision may have only been an apparent cause of the calving as other factors had not been fully considered such as seafloor interactions (Massom et al., 2015; Wang. 2014). By comparing inverted ice thickness to surrounding bathymetry, and combining remote sensing analysis, Massom et al., (2015) considered that the seabed contact may have held the glacier tongue in place to delay calving by ~8 years. The interaction of the MIT with seafloor, the exact grounding location of the MIT before calving and the extent of grounding are still not well-known.

The MIT (66°S-68°S, 144°E-150°E, Fig. 1), located in King George V Land, East Antarctica, extended over 140 km from its grounding line to the tongue front and is approximately 30 km wide at the front (Legresy et al., 2004). Much field exploration has been conducted around Mertz and the increasing availability over the last decade of remote sensing, hydrographic surveying, and bathymetric data allows to investigate the mechanism of the ice tongue instability and calving. From satellite altimetry, a modest elevation change rate of 0.03 m/a (Pritchard et al., 2012) and a freeboard change rate of -0.06 m/a (Wang et al., 2014) were

found, which implied that the combined effects of surface accumulation and basal melt were not dramatic for this ice tongue. Investigations of tidal effects, surface velocity, rift propagation, and ice front propagation (Berthier et al., 2003; Frezzotti et al., 1998; Legresy et al., 2004; Lescarmontier et al., 2012; Massom et al., 2010, 2015) have been conducted with an objective of detecting underlying factors affecting the stability of the MIT. Grounding has been suggested as a potential mechanism to affect the stability of the MIT by delaying calving (Massom et al. 2015). However, without highly accurate bathymetric data, it is impossible to carry out such a study. Fortunately, In 2010, a new and high resolution bathymetry model, with a resolution of 100 m was released for the Terra Adelie and George V continental margin (Beaman et al., 2011), and it has later been used to generate Bedmap-2 (Fretwell et al., 2013). This accurate data set (Fig 3) provides an opportunity for better exploring seafloor shoals and their impacts on the instability of the MIT. In this study, we focus on grounding events of the MIT from 2002 to 2008. A method for grounding detection is proposed and grounding of the MIT before the calving is investigated. A calving cycle of the MIT caused by grounding on seafloor shoal, Mertz Bank is discussed as well.

2. Data

The primary data used to investigate grounding of the MIT in this study are elevation data from Geoscience Laser Altimeter System (GLAS) onboard the Ice, Cloud and land Elevation Satellite (ICESat) and the seafloor bathymetry data mentioned above. In this section, the ICESat/GLAS and bathymetry data, as well as some preprocessing are introduced.

2.1 ICESat/GLAS

ICESat is the first spacebone laser altimetry satellite orbiting the Earth, launched by the National Aeronautics and Space Administration (NASA) in 2003 (Zwally et al. 2002) with

GLAS as the primary payload onboard. ICESat/GLAS was operated in an orbit of ~600 km and had a geographical coverage from 86 º S to 86 º N. ICESat/GLAS usually observed in nadir viewing geometry and employed laser pulses of both 532 nm and 1064 nm to measure the distance from the sensor to ground (Zwally et al. 2002). On the ground, ICESat/GLAS's footprint covered an area of approximately 70 m in diameter, with adjacent footprints spaced by ~170 m. The horizontal location accuracy of the footprint was approximately 6 m (Abshire et al. 2005). The accuracy and precision of ICESat/GLAS altimetry data were 14 cm and 2 cm respectively (Shuman et al. 2006). ICESat/GLAS usually made two or three campaigns a year from 2003 to the end of 2009, each campaign lasted for approximately one month. 15 different types of data were produced for various scientific applications, named as GLA01, GLA02, … GLA15. In this study, GLA12 data (elevation data for polar ice sheet) covering Mertz from release 33 between 2003 and 2009 is used (Fig. 2).

2.2 Seafloor Topography

Detailed bathymetry maps are fundamental spatial data for marine science studies (Beaman et al., 2003, 2011) and crucially needed in the data-sparse Antarctic coastal region (Massom et al. 2015). Regionally, around Mertz, a large archive of ship track single-beam and multi-beam bathymetry data from 2000 to 2008 were used to generate a high resolution Digital Elevation Model (DEM) for which the spatial coverage can be found in Figs. 3(b) and 3(c). The DEM product was reported to have a vertical accuracy of approximately 11.5 m (500 m depth) and a horizontal accuracy of 70 m (500 m depth) in the poorest situation (Beaman et al. 2011). As can be seen from Figs. 3(b) and 3(c), there is no bathymetry data under the MIT, which may result in large uncertainty for seafloor interpolation. The oldest bathymetry data collected along the margin of the MIT was from 2000 (Beaman et al. 2011). Additionally, around the Mertz ice

front, for both the east and west flanks, bathymetry data does exist. Since the ice front has a width of ~34 km (Wang et al. 2014), the accuracy of seafloor DEM under the MIT varies depending on distance to margin. Inside the 2000 boundary of the MIT, the closer to the dash-dotted polygon (Figs. 6 and 7), the better accuracy the seafloor DEM. Outside of that boundary, the quality of the seafloor DEM data is much better because of high density of single-beam or multi-beam bathymetric measurements.

Around Antarctica, the seafloor topography data from Bedmap-2 was produced by Fretwell et al. (2013) which adopted the DEM from Beaman et al. (2011). In this study, Bedmap-2 seafloor topography data covering Mertz is employed to detect the contact between seafloor and the MIT. Because of inconsistent elevation systems for ICESat/GLAS and the seafloor topography data, the Earth Gravitational Model 2008 (EGM08) geoid (Pavlis et al. 2012) with respect to World Geodetic System 1984 (WGS-84) ellipsoid is taken as reference. Since the seafloor topography from Bedmap-2 is referenced to the so-called g104c geoid, an elevation transformation is required and can be implemented through:

$$E_{sf} = E_{seafloor} + gl04c_{to\_wgs84} - EGM2008 \quad (1)$$

where E_{sf} and $E_{seafloor}$ is the seafloor topography under the EGM08 and g104c geoid respectively, $gl04c_{to\_wgs84}$ is the value needed to convert height relative to the gl04c geoid to that under the WGS-84, and *EGM2008* is the geoid undulation with respect to the WGS-84.

3. Methods

3.1 Grounding Detection Methods

ICESat/GLAS data has been widely used to determine ice freeboard, or ice thickness, since its launch in 2003 (Kwok et al., 2007; Wang et al., 2011, 2014; Yi et al., 2011; Zwally et al., 2002, 2008). The methods we designed for grounding detection of the MIT using the

ICESat/GLAS data are introduced here. First, assuming a floating MIT, based on freeboard data extracted in different observation dates, ice draft of the MIT is inverted. Next, ice bottom elevation is calculated based on the inverted ice draft and the lowest sea-surface height. Finally, the ice bottom is compared with seafloor bathymetry to detect ice grounding. The underlying logic for grounding detection is that if the inverted ice bottom is lower than seafloor, we can draw a conclusion that the ice tongue is grounding rather than floating.

The method for extracting a freeboard map using ICESat/GLAS from multiple campaigns over the MIT was described in Wang et al. (2014). Without providing details, here we only introduce it schematically. Four steps are included in freeboard map production for each of the datasets from November 14, 2002, March 8, 2004, December 27, 2006 and January 31, 2008.

The first step involves data preprocessing, saturation correction, data quality control, and tidal correction removal. The magnitude of the ICESat/GLAS waveform can become saturated because of different gain setting, or high reflection from natural surfaces. Thus, saturated waveforms with *i_satElevCorr* (i.e. an attribute from GLA12 data record) greater than or equal to 0.50 m are ignored and only those measurements with *i_satElevCorr* less than 0.50 m are corrected following the procedures in Wang et al. (2012, 2013). Additionally, measurements with *i_reflctUC* greater than or equal to one are ignored. Furthermore, the tidal correction from TPX07.1 tide model in GLA12 data record is removed to obtain estimates for the instantaneous sea surface height. Finally, elevation data from ICESat/GLAS related to the WGS-84 ellipsoid and EGM 08 geoid from 2003 to 2009 is available for subsequent use.

The second step is to derive sea-surface height according to each track and to calculate freeboard for each campaign. Because of tidal variations near the MIT, surface elevations of the MIT can vary as well. To derive sea-surface height from ICESat/GLAS and provide a reference

for freeboard calculation for different campaigns, the ICESat/GLAS data over the MIT within a buffer region (with 10 km as buffer radius of MIT boundary in 2007) are selected and sea-surface height is determined as the lowest elevation measurement along each track (Wang et al. 2014). Freeboard is then calculated by subtracting the corresponding sea-surface height from elevation measurements of the MIT according to different tracks from the same campaign. Thus freeboard data for different campaigns from 2003 to 2009 is obtained.

The third step is to relocate footprints using estimated ice velocity. ICESat observed the MIT almost repeatedly along different tracks in different campaigns (Fig. 2). However, observations from only one campaign cannot provide good coverage of the MIT. All observations from 2003 to 2009 are combined together to produce a freeboard map of the MIT. Fig. 2 shows the spatial coverage of ICESat/GLAS from 2003 to 2009 over Mertz, but the geometric relation between tracks is not correct over the MIT because the tongue was fast moving and observed in different years by ICESat. Regions observed in an earlier campaign would move downstream later (Wang et al. 2014). For example, consider ICESat data from track T31 from March 22, 2003 and T165 (Fig. 2) from November 1, 2003 respectively. Fig. 2 shows that the distance between track T165 and T31 is ~7.5 km without accounting for ice advection between observation dates. However because of the fast moving ice tongue, the distance of their actual ground tracks on surface of the MIT should be longer because T165 was located upstream and observed later. Thus footprints relocation using ice velocity is critical to obtain accurate geometric relations among different tracks. The ice velocity data from Rignot et al. (2011) generated from InSAR data from 2006 to 2010 is used to relocate the footprints of ICESat/GLAS. The correct geospatial relations between observations from different campaigns can be achieved on November 14, 2002, March 8, 2004, December 27, 2006, and January 31, 2008, through:

$$X = x + \sum_{i=1}^{n} v_{xi}\Delta t + v_{xm}t_m \quad (2)$$

$$Y = y + \sum_{i=1}^{n} v_{yi}\Delta t + v_{ym}t_m \qquad (t_m = t_2 - t_1 - n\Delta t) \quad (3)$$

where x and y are the horizontal positions directly from the ICESat measurements, and X and Y are the horizontal positions after relocation respectively; v_x and v_y are the horizontal components of the ice velocities; t_1 and t_2 are the start and end times; Δt is the time interval and n indicates the largest integer time steps for time interval between t_1 and t_2; t_m is the residual time; In this work, Δt is set as 10 days; v_{xi} and v_{yi} is derived from ice velocity field according to different locations during relocation and may change in different time intervals.

Freeboard changes with time should be considered as well, but it is neglected because comparison of freeboard from crossing tracks showed a slightly decreasing trend of -0.06 m/a on average (Wang et al. 2014). The spatial distribution of freeboard data over the MIT for November 14, 2002, is shown in Fig. 5(a).

The forth step is to interpolate freeboard map using the relocated freeboard data from the third step. Kriging interpolation in ArcGIS is selected in this study to produce freeboard maps of the MIT because it can provide an optimal interpolation estimate for a given coordinate location by considering the spatial relationships of a data set. With this method, freeboard maps of the MIT are produced for November 14, 2002, March 8, 2004, December 27, 2006, and January 31, 2008 respectively when the ice tongue outline can be delineated from Landsat images.

Ice draft is calculated with Eq. (4) assuming hydrostatic equilibrium and using the lowest sea-surface height E_{sea_level} as reference for the sea surface elevation.

$$\rho_w D = \rho_i (H_f + D - FAC) \quad (4)$$

where D is the ice draft, i.e. vertical distance from the sea surface to the bottom of the ice; H_f is the freeboard, i.e. the vertical distance from the sea surface to the top of the snow; ρ_w and

195 ρ_i are the densities of ocean water and ice, respectively. In this study, the ice and sea water
196 density are taken as 915 kg/m^3 and 1024 kg/m^3, respectively (Wang et al., 2014); FAC is the firn
197 air content which corresponds to the decrease in thickness (in meters) that occurs when the firn
198 column is compressed to the density of glacier ice, as defined in Holland et al., (2011) and
199 Ligtenberg et al. (2014).

200 The sea surface is taken as the lowest sea surface height (E_{sea_level}) and is derived from
201 the minimum of all sea surface heights from the different ICESat/GLAS tracks between 2003
202 and 2009 and amounts in our case to -3.35 m. For time varying sea-surface heights caused by
203 tides, the minimum sea-surface height can allow ice with a given draft to ground to the seafloor.
204 Then, the ice bottom elevation is calculated by considering the ice draft and the lowest sea-
205 surface height. Elevation difference of the ice bottom and the seafloor is calculated. A negative
206 value indicates that the ice bottom is lower than the seafloor, which suggests grounding.

207 The elevation of the underside (bottom) of the tongue E_{ice_bottom} is calculated from:

208 $$E_{ice\_bottom} = E_{sea\_level} - D \quad (5)$$

209 Similarly, the elevation difference of ice tongue bottom and seafloor is defined as E_{dif},
210 which can be calculated by:

211 $$E_{dif} = E_{ice\_bottom} - E_{sf} \quad (6)$$

212 where E_{sf} is the seafloor elevation as defined in Eq. (1).

213 **3.2. Firn Air Content Estimation Method**

214 The Antarctic ice sheet is covered by a dry, thick firn layer which represents an
215 intermediate stage between fresh snow and glacial ice, having varying density from Antarctic
216 inland to the coast (van den Broeke, 2008). The density and depth of the Antarctic firn layer has
217 been modeled (e.g., van den Broeke, 2008) using a combination of regional climate model output

and a steady-state firn compaction model. However, for ice thickness inversion, Firn Air Content (FAC) is usually used to make the calculation convenient (Rignot and Jacobs. 2002). FAC is defined as the decrease in thickness (in meters) that occurs when the firn column is compressed to the density of glacier ice (Holland et al., 2011). Time-dependent FAC has also been modeled by considering the physical process of the firn layer (e.g., Ligtenberg et al. 2014). For the MIT, there are some in-situ measurements of snow thickness available from Massom et al. (2010) who used a snow layer depth of 1 m to derive the thickness of surrounding multi-year, fast sea ice. However on the surface of the MIT, no in-situ measurements of density or depth of firn layer are available.

Because of different density and thickness of the firn layer on the top of an ice tongue, it is challenging to simulate the density profile of the MIT without in-situ measurements as control points. In this study, we use FAC extracted from adjacent seafloor-touching icebergs rather than that from modeling to investigate the grounding of the MIT. The MIT may be composed of pure ice, water, air, firn or snow that will influence the density of the ice tongue. However, if assuming a pure ice density only to calculate ice mass, the thickness of MIT must be corrected by the FAC. The FAC can be inferred from surrounding icebergs that are slightly grounded under the assumption of hydrostatic equilibrium and known ice draft and freeboard. It is, however, critical to target and use icebergs that fulfil the condition of slight grounding. From Smith (2011), icebergs can be divided into three categories based on bathymetry and seasonal pack ice distributions: grounded, constrained, and free-drifting icebergs. Without pack ice, an iceberg can be free-drifting or grounded. Free-drifting icebergs can move several tens of kilometers a day, such as iceberg A-52 (Smith et al. 2007). Grounded icebergs can be heavily or lightly anchored. Heavily grounded icebergs have firm contact with the seafloor and can be kept

241 stationary for a long time, such as iceberg B-9B (Massom. 2003). However, slightly grounded
242 icebergs may have less contact with the seafloor and can possibly move slowly under the
243 influence of ocean tide, ocean currents, or winds, but much slower than free-drifting icebergs.
244 The relation of grounded iceberg to the drifting velocity is not well-known. However, slowly
245 drifting or nearly stationary icebergs in open water are good indicators for slight grounding and
246 therefore are used to infer FAC.

247 Because of the heavily grounded iceberg B-9B to the east of the MIT blocking the
248 drifting of pack ice or icebergs from the east, icebergs located between B-9B and the MIT are
249 most likely generated from the Mertz or Ninnis glaciers. Some icebergs may be slightly
250 grounded as can be detected from remote sensing. We calculate the FAC from these slightly
251 grounded icebergs and later apply it to grounding event detection of the MIT. Around the MIT,
252 the locations of three icebergs ('A', 'B' and 'C') were investigated using MODIS and Landsat
253 images in austral summer of 2006 and 2008 respectively and shown in Fig. 4. Fortunately,
254 ICESat/GLAS observed these icebergs on February 23, 2006 (54th day of 2006) and February 18,
255 2008 (49th day of 2008) which allows us to analyze the behavior of these icebergs three-
256 dimensionally. Fig. 4a shows that icebergs 'A', 'B' and 'C' were almost stagnant and only
257 slightly changed their positions and orientation over two months (from 28 to 85 day of 2006).
258 Thus we can consider these icebergs slightly grounded. For these slightly grounded icebergs,
259 hydrostatic equilibrium should still apply, so the ice draft inverted from freeboard measurement
260 assuming hydrostatic equilibrium should be equal to the water depth. Based on this analysis, we
261 can take water depth as the draft to calculate the FAC.

262 Because only icebergs 'A' and 'C' were observed by track T1289 of ICESat/GLAS in
263 2006, the FAC is inverted using freeboard and water depth from bathymetry from both

icebergs(Figs. 3b, 3c, 4, and Table 1). However, the icebergs were not stationary, which indicates that only some parts were slightly grounded. Therefore, only the top two largest freeboard measurements of icebergs 'A' and 'C' from T1289 in 2006 are used to calculate the FAC with Eq. (7) with a least-squares method under hydrostatic equilibrium.

$$FAC = H_{f\_k} + D_k - \frac{\rho_w}{\rho_i} D_k + \varepsilon_k \quad (7)$$

where k refers to the icebergs 'A' or 'C', H_f is the top two largest freeboard measurement of each iceberg, D is the ice draft which is the same as sea water depth and is taken from the seafloor bathymetry directly, ε is the residual of FAC.

Table 1 shows the freeboard of iceberg 'A' and 'C' from 2006 and seafloor bathymetry for FAC inversion and grounding detection of icebergs 'A' and 'B' in 2008 (detailed freeboard values for these icebergs can be found from S-Fig. 1). With the freeboard from 2006 and seafloor bathymetry (Table 1), the FAC is calculated as 4.87 ±1.31 m. Icebergs 'A' and 'B' were observed by the same track T1289 on February 18, 2008 and thus are taken to evaluate the grounding detection by using the inverted FAC. From iceberg trajectories observed by remote sensing (Fig. 4b), we know, iceberg 'A' drifted away from its original position. Thus it was not grounded. However, iceberg 'B' were kept rotating in this period without drifting away, indicating a slight grounding. Such grounding status determined from remote sensing can also be detected with our method since the elevation difference of the ice bottom and seafloor from Table 1 does clearly indicate a slightly grounded iceberg 'B' and a floating iceberg 'A'. Thus, our FAC estimation works well around Mertz.

FAC varies across the Antarctica ice sheet, usually decreasing from the interior to the coast. For Mertz we obtain a FAC of 4.87 ±1.31 m. Other studies, using a time variable approach, modelled FAC values between 5 and 10 m (Ligtenberg et al. 2014) and in the absence of in-situ

measurements our estimate seems consistent, but there are some shortcomings which should be further explored.

First, for FAC calculation, icebergs just touching the seafloor should be used in which case the FAC calculated assuming hydrostatic equilibrium is the same as its actual value. However, it is difficult to ascertain whether an iceberg is just touching the seafloor from remote sensing images. The near stationary or slowly rotating icebergs detected with remote sensing may be grounded more than just touching the seafloor, which may result in a inverted FAC theoretically greater than its actual value. Thus, using this FAC value to detect grounding can potentially lead to smaller grounding results. However, once a grounded iceberg or ice tongue is detected using this FAC, the result is more convincing.

Second, limited observations from ICESat/GLAS may not catch the same and the thickest section of a slight grounding iceberg. Because ICESat/GLAS observed only several times a year on repeat tracks and icebergs were rotating slowly, the elevation profile in 2006 and 2008 along the same track T1289 may not refer to the same ground surface. S-Fig. 1 shows the freeboard of icebergs ‘A’, ‘B’ and ‘C’ derived from ICESat/GLAS from 2006 and 2008 respectively. By comparing the freeboard of iceberg ‘A’ in 2006 (S-Fig. 1a), and 2008 (S-Fig. 1c), we find the larger freeboard and the longer freeboard profile in 2006. Comparatively, the smaller freeboard in 2008 may be caused by basal melting or observing a different portion of iceberg ‘A’ by ICESat. Since the larger freeboard measured in 2006 indicates a high possibility of capturing the thickest portion, it is reasonable to use it to invert the FAC. Additionally, icebergs ‘A’ and ‘C’ did show a similar maximum freeboard (Table 1), which is another important reason to select the measurements of 2006 for the inversion.

4. Accuracy of Grounding Detection

The accuracy of E_{dif} is critical to grounding detection of the MIT. From Eq. (1) to (6), we find different components of error sources, such as from sea surface height determination, ice draft, seafloor bathymetry, and elevation transformation. Meanwhile, the uncertainty of ice draft is primarily depending on that of freeboard and *FAC*. Furthermore, the uncertainty of freeboard is influenced by the footprint relocation and freeboard changing rates. Considering all that mentioned above, the error sources of elevation difference E_{dif} can be synthesized by:

$$\Delta E_{dif} = \Delta E_{sl} + a(\Delta H_f + \Delta E_{re} + \Delta E_{fb_c} + \Delta FAC + \Delta E_{krig}) + \Delta E_{sf} + \Delta E_{trans} \quad (8)$$

where $a = \frac{\rho_i}{\rho_w - \rho_i}$; Δ stands for error of each variable; ΔE_{dif} stands for the error of the final elevation difference of ice bottom and seafloor; ΔE_{sl}, ΔH_f, ΔE_{re}, ΔE_{fb_c}, ΔFAC, ΔE_{sf}, ΔE_{krig}, and ΔE_{trans} stand for errors caused by the sea surface height extraction, freeboard extraction, freeboard relocation, freeboard changing rates, FAC calculation, seafloor bathymetry, kriging interpolation and elevation system transformation, respectively.

The influence of elevation system transformation on final elevation difference can be neglected. Based on the error propagation, the uncertainty of elevation difference E_{dif} can be described by:

$$\varepsilon E_{dif} = \sqrt{(\varepsilon E_{sl})^2 + a^2[(\varepsilon H_f)^2 + (\varepsilon E_{re})^2 + (\varepsilon E_{fb_c})^2 + (\varepsilon FAC)^2 + \left(\varepsilon E_{krig}\right)^2] + (\varepsilon E_{sf})^2} \quad (9)$$

where ε indicates the uncertainty of each parameter.

4.1 Uncertainty of Kriging Interpolation

Fig. 5a shows the spatial distribution of freeboard data over the MIT used for grounding detection from November 14, 2002. The spatial difference of the ICESat/GLAS data between Fig. 2 and Fig. 5 is caused by the footprint relocation, after which the spatial geometry between

different tracks is reasonably correct. In the lower right of the Mertz ice front (Fig. 5a), the crossing-track distance between T1289 and T165 is approximately 7 km. In these data gaps, the freeboard data used for grounding detection is interpolated using kriging. Thus, knowing the uncertainty of kriging interpolation is critical to the final grounding detection.

To investigate the uncertainty of kriging interpolation method, freeboard measurements from ICESat/GLAS should be compared with the interpolated freeboard estimates. A testing region with freeboard measurements is selected (dashed blue square in Fig. 5a, 7 km×7 km in size). A freeboard map is first interpolated with the gray dots (Fig. 5a) using kriging. The freeboard measurements (284 of green dots in Fig. 5a) are then compared with the interpolation from the square. The spatial distribution and the histogram of freeboard difference derived by subtracting the krigged freeboard from the freeboard derived from ICESat/GLAS are shown in Fig. 5b.

The freeboard measurement varies from 31.6 m to 40.0 m with an average of 36.6 m. However, the interpolated freeboard varies from 32.9 m to 39.6 m with an average of 35.9 m. From the freeboard difference (Fig. 5b), we find that the interpolated freeboard shows similar results compared with the freeboard derived from ICESat/GLAS. The interpolated freeboard has an accuracy of -0.7 ± 1.8 m indicating that the interpolated freeboard using kriging can reflect the actual freeboard well.

4.2 Grounding Detection Robustness

Since the sea surface height is extracted from the ICESat/GLAS data track by track, we use ±0.15 m (Zwally et al. 2002) as the uncertainty of elevation data (εE_{sl}). Also from Wang et al. (2014), we can find that the uncertainty of freeboard extraction (εH_f) was ±0.50 m. From Rignot et al. (2011), the error of the ice velocity ranged from 5 m/a to 17 m/a. Assuming that the

ice velocity varied by 17 m/a (an upper threshold), the relocation error horizontally could reach ±54 m when considering a three-year period. Wang et al. (2014) extracted the average slope of the MIT along the ice flow direction as 0.00024. However, because of large crevasses on the surface, we use 50 times of this value as a conservative estimate of the average slope. In this way, we can estimate εE_{re} as ±0.65 m when considering a three-year period. The annual rate of freeboard changes from 2003 to 2009 was -0.06 m/a (Wang et al. 2014). Therefore, we consider the freeboard stable over this period. However when combining data from different time periods, εE_{fb_c} is estimated to be ±0.18 m. From Beaman et al. (2011), considering the elevation uncertainty at the worst situation when water depth reaches 500 m, εE_{g104c} is ±11.5 m. Using Eq. (9) and kriging interpolation, from the analysis from Section 4.1, 1.8 m is taken as the uncertainty. Using all these errors above, we calculate the final uncertainty of the elevation difference as ± 23 m.

From the calculations above, a less than -23 m E_{dif} indicates a robust grounding event. However, if E_{dif} is greater than 23 m, grounding cannot be confirmed. E_{dif} between -23 m and 23 m corresponds to slight grounding or floating. We can also determine different contributions of each separate factor to the overall accuracy. Seafloor bathymetry contributes the greatest part and is the dominant factor affecting the accuracy of grounding detection.

5. Grounding Detection Results

The spatial distribution of the elevation difference E_{dif} and the outlines of the MIT from 2002 to 2008 are shown in Fig. 6. Since the moving trajectory of the Mertz ice front changed by more than 40 degrees clockwise (Massom et al. 2015; Wang. 2014), a buffer region with radius of 2 km (region between black and grey lines in Fig. 6) is introduced to investigate grounding potential of the MIT. The freeboard in the buffer region is extrapolated using the kriging

interpolation method and the elevation difference is calculated. The elevation difference less than 46 m (twice the uncertainty of the elevation difference εE_{dif}) both inside and outside the outline is extracted and the statistics are shown in Table 2. Since the uncertainty to determine a grounding event is $\pm$23m, if some grids of the MIT have elevation difference E_{dif} less than -23 m, we can conclude that this section of the tongue is strongly grounded. The smaller the E_{dif}, the more robust the grounding.

As illustrated in Table 2 and Fig 6, the minimum E_{dif} inside the MIT in 2002 was 11.9 m and the minimum E_{dif} inside the MIT was less than -23 m after 2002. The minimum E_{dif} in the buffer region were all less than -23 m from 2002 to 2008. This suggests that the MIT had grounded on the shallow Mertz Bank at least since November 14, 2002. This result coincides with the findings from Massom et al. (2015) who considered that the northwestern extremity of the MIT started to touch a seafloor shoal in late 2002 to early 2003. Also, it would have been difficult for the MIT to approach the buffer region (indicated with yellow to red colors in Fig. 6) as the surrounding Mertz Bank gets shallower and steeper, suggesting substantive grounding potentials. Inside the MIT, the minimum E_{dif} was just 11.9 m on November 14, 2002, which indicates slight grounding. However on March 8, 2004, December 27, 2006, and January 31, 2008, the minimum E_{dif} reached -46.0 m, -52.3 m and -34.8m respectively, which indicates that strong grounding occurred in some regions. From 2002 to 2008, more regions under the MIT had E_{dif} less than 46 m, the area of which increased from 8 km^2 to 17 km^2. Additionally, the mean of those E_{dif} less than 46 m gradually decreased from 28.8 m to 12.3m, according to which we can conclude that the ice front became more firmly grounded as time passed on. Since the grounding area increased from 8 km^2 to 17 km^2 (Table 2) and the mean of E_{dif} decreased, we

conclude that during the period from 2002 to 2008, the grounding of the northwest tip of the MIT became more widespread.

Based on the calculated elevation difference, the grounding outlines of the MIT are delineated for November 14, 2002, March 8, 2004, December 27, 2006 and January 31, 2008 respectively (Fig. 7). For the grounded part of the outlines in different years, the starting and ending location and the perimeter are also extracted (Table 3), from which we conclude that the length of the grounding outline on the Mertz Bank was only limited to a few kilometers. We find that the lower right (northwest) section of the MIT was always grounded and grounding did not occur in other regions (Fig. 6). The shallowest seafloor that the Mertz ice front touched was ~ -290 m in November 2002. In 2004, 2006, and 2008, the lower right (northwest) of the MIT even approached the contour of -220 m.

6. Discussion

6.1 Area Changing Rate and ~70-year Calving Cycle of MIT

Using Landsat TM/ETM+ images from 1989 to 2013, outlines of the MIT are extracted manually. Assuming a fixed grounding line position, the area of the MIT over this period is calculated. Using these data, from 1989 to 2007, an increasing are-change trend of the MIT was obtained (from 5453 km^2 to 6126 km^2) in Fig. 8. However, the area of the MIT was almost constant from 2007 to 2010, before calving. The largest area of the MIT was 6113 km^2 closest to the calving event in 2010. After the calving, the area decreased to 3617 km^2 in November 2010.

The average area-change trend of the MIT from 1989 to 2007 was also obtained using a least-squares method, corresponding to 35.3 km^2/a. However, after the calving a slightly higher area-change trend of 36.9 km^2/a, was found (Fig. 8). On average, the area-change trend of the MIT was approximately 36 km^2/a.

The surface dynamics of the MIT such as ice flow direction changes and middle rift changes caused by grounding was analyzed by Massom et al. (2015). In the history of the MIT, one or two large calving events were suspected to have happened between 1912 and 1956 (Frezzotti et al., 1998). Based on the interactions between the MIT and Mertz Bank suggested by our observations and description below, it is likely that only one large calving event occurred between 1912 and 1956. When the MIT touched Mertz Bank, the bank started to affect its stability by bending it clockwise to the east, as can be found from velocity changes from Massom et al. (2015). With continuous advection of the ice and flux input from the upstream, a large rift from the west flank of the tongue would ultimately have to occur and could potentially calve the MIT. A sudden length shortening of the MIT can be caused by such ice tongue calving as indeed had happened in February, 2010. We also consider that even without a sudden collision of iceberg B-9B in 2010, the MIT would eventually have calved because of the effect of the shallow Mertz Bank.

When considering 6127 km^2 as the maximum area of the MIT and assuming a constant area-changing trend of 36.9 km^2/a after 2010, the MIT will take approximately 68 years to calve again. When assuming an area changing trend of 35.3 km^2/a as before 2010, the MIT will take a little longer, approximately 71 years to calve. Therefore, without considering an accidental collision with other large icebergs, the MIT is predicted to calve again in ~70 years. Because of continuous advection of the ice from upstream and the fixed location of the shallow Mertz Bank, the calving is likely repeatable and a cycle therefore exists.

After the MIT calved in February, 2010, the Mertz polynya size, sea-ice production, sea-ice coverage and high-salinity shelf water formation changed as well. A sea-ice production decrease of approximately 14-20% was found by Tamura et al. (2012) using satellite data and the

high-salinity shelf water export was reported to reduce up to 23% using a state-of-the-art ice-ocean model (Kusahara et al. 2010). Recently, Campagne et al. (2015) pointed out a ~70-year cycle of surface ocean condition and high-salinity shelf water production around the Mertz through analyzing some reconstructed sea ice and ocean data over the last 250 years. They also mentioned that this cycle was closely related to the presence and activity of the Mertz polynya. However, the reason for this cycle was not fully understood.

From these findings addressed above and the MIT calving cycle we find that the calving cycle of the MIT leads to the ~70-year cycle of surface ocean condition and high-salinity shelf water production around the Mertz. Variations in length of the MIT will prevent sea ice drifting from the east side to a variable degree. A long MIT contributes to maintain a large polynya because sea ice from the east side cannot drift to the west side. The sea ice produced on the west side is blown seaward by the katabatic wind and thereby maintains a polynya and stable sea ice production. The sudden shortening of the MIT after a calving event therefore reduces the size of Mertz Polynya formed by Antarctic katabatic winds, resulting in a lower sea-ice production and further lessens high-salinity shelf water production. Therefore, the cycle of ocean conditions around the Mertz found by Campagne et al. (2015) is likely dominated by the calving of the MIT. Additionally, the 70-year cycle of the MIT calving coincides well with the change of surface ocean condition around the Mertz which makes the explanation much more compelling.

6.2 Seafloor DEM

High accuracy seafloor is critical to the final success of the grounding detection. According to our best knowledge, Beaman et al. (2011) provided the most accurate seafloor DEM over the Mertz, so the seafloor DEM inside dash-dotted polygon (Fig. 7) was kept and the grounding detection was conducted there (Fig. 6). Additionally, the ice tongue continued to

advance out into the ocean, where the bathymetry observation density is good. From the results shown in Fig. 6 all grounding sections of the MIT boundary were located outside of the 2000 boundary. Thus the analysis of the grounding detection near the ice front in 2002, 2004, 2006, and 2008 is convincing. Inside the 2000 boundary, most of the grounding detection results were above 100 m, indicating a floating status of the corresponding ice. Only abnormal seafloor features higher than this seafloor DEM by more than 100 m could result in wide grounding inside. Actually, no matter whether the MIT inside the 2000 boundary was grounded or not, gradual grounding on the shallow Mertz Bank of the MIT since late 2002 is well supported by observations and which we take as evidence to infer the primary cause of the instability of the MIT.

6.3 Influence of Mertz Bank on MIT

Fig. 7 shows the extension line of the west flank in November, 2002, from which we can find that if the MIT advected along the former direction, the ice flow would be seriously obstructed when approaching the Mertz Bank. The shallowest region of the Mertz Bank has an elevation of approximately -140 m and the MIT would have to climb the 140 m obstacle to cross it. The shallow Mertz Bank would have caused strong grounding during the climbing. This special feature of the seafloor shoal facing the MIT can further explain why the ice velocity differed along the east and west flanks of the MIT before calving and why the ice tongue was deflected clockwise to the east, as suggested by Massom et al. (2015). However, because of sparsely-distributed bathymetric data in the Mertz region used in Massom et al. (2015), this effect could not be easily seen. Here, from our grounding detection results and surrounding high-accuracy bathymetry data, this effect is more clearly observed.

7. Conclusion

In this study, a method of FAC calculation from seafloor-touching icebergs around the Mertz region is presented as an important element in understanding the MIT grounding. The FAC around the Mertz is 4.87 ±1.31 m. This FAC is used to calculate ice draft based on the sea surface height and freeboard extracted from ICESat/GLAS and is performing well. A method to extract the grounding sections of the MIT is described based on comparison of the inverted ice draft assuming hydrostatic equilibrium with the seafloor bathymetry. The final grounding results explain the dynamic behavior of the MIT. Previous work by Massom et al. (2015) has also provided some evidence for seafloor interaction, in showing that the MIT front had an approximate 280 m draft with the nearby seafloor as shallow as 285 m, suggesting the possibility of grounding. In our work, we have provided ample detailed bathymetry and ice draft calculations. Specifically, the ice bottom elevation of the MIT is inverted using the ICESat/GLAS data and compared with seafloor bathymetry from 2002, 2004, 2006, and 2008 respectively. From these calculations we show conclusively that the MIT was indeed grounded along a specific portion of its northwest tip over a limited region. We also point out that even without collision by iceberg B-9B in early 2010 the ice tongue would eventually have calved because of the ice advection from the upstream and the glacier flow increasingly diverted by the obstructing seafloor shoal of the Mertz Bank.

From remote sensing images we are able to quantify the trend of area increase of the MIT before and after the 2010 calving. While the area-increase trend of the MIT after calving was slightly greater than that before, we use the averaged trend to estimate a timescale required for the MIT to re-advance to the area of the shoaling bathymetry from its retreated, calved position. Our estimate is ~70-years, which is remarkably consistent with Campagne et al. (2015) who found a similar period for variations in sea surface conditions using seafloor sediment data. Thus,

514 the shoaling on the Mertz Bank combined with the rate of advancing of the MIT determines the
515 70-year repeat cycle. Also the calving cycle of the MIT explains the observed cycle of the sea-
516 surface conditions change well, which indicates that the calving of the MIT is the dominant
517 factor for the sea-surface condition change. Understanding the mechanism underlying the
518 periodicity of the MIT calving is important as the presence or absence of the MIT has a profound
519 impact on the sea ice and hence of the bottom water formation in the local region.

520 **Acknowledgements**

521 This research was supported by the Center for Global Sea Level Change (CSLC) of NYU
522 Abu Dhabi (Grant: G1204), the Open Fund of State Key Laboratory of Remote Sensing Science
523 (Grant: OFSLRSS201414), the China Postdoctoral Science Foundation (Grant: 2012M520185,
524 2013T60077) and Fundamental Research Fund for the Central University. We are grateful to the
525 Chinese Arctic and Antarctic Administration, the European Space Agency for free data supply
526 under project C1F.18243, the National Snow and Ice Data Center (NSIDC) for the availability of
527 the ICESat/GLAS data (http://nsidc.org/data/order/icesat-glas-subsetter) and MODIS image
528 archive over the Mertz glacier (http://nsidc.org/cgi-bin/modis_iceshelf_archive.pl), British
529 Antarctica Survey for providing Bedmap-2 seafloor topography data
530 (https://secure.antarctica.ac.uk/data/bedmap2/), the National Geospatial-Intelligence Agency for
531 publicly released EGM2008 GIS data (http://earth-
532 info.nga.mil/GandG/wgs84/gravitymod/egm2008/egm08_gis.html), and the USGS for Landsat
533 data (http://glovis.usgs.gov/). Fruitful discussions with M. Depoorter, P. Morin, T. Scambos and
534 R. Warner, and constructive suggestions from Editor Andreas Vieli and two anonymous
535 reviewers are acknowledged.

536 **References**

1. Abshire, J. B., Sun, X., Riris, H., Sirota, J. M., McGarry, J. F., Palm, S., ... & Liiva, P. (2005). Geoscience laser altimeter system (GLAS) on the ICESat mission: on ‐ orbit measurement performance. *Geophysical Research Letters*, 32(21).
2. Beaman, R. J., & Harris, P. T. (2003). Seafloor morphology and acoustic facies of the George V Land shelf. *Deep Sea Research Part II: Topical Studies in Oceanography*, 50(8), 1343-1355.
3. Beaman, R. J., O'Brien, P. E., Post, A. L., & De Santis, L. (2011). A new high-resolution bathymetry model for the Terre Adélie and George V continental margin, East Antarctica. *Antarctic Science*, 23(01), 95-103.
4. Berthier, E., Raup, B., & Scambos, T. (2003). New velocity map and mass-balance estimate of Mertz Glacier, East Antarctica, derived from Landsat sequential imagery. *Journal of Glaciology*, 49(167), 503-511.
5. Campagne, P., Crosta, X., Houssais, M. N., Swingedouw, D., Schmidt, S., Martin, A., ... & Massé, G. (2015). Glacial ice and atmospheric forcing on the Mertz Glacier Polynya over the past 250 years. *Nature Communications*, 6.
6. Depoorter, M. A., Bamber, J. L., Griggs, J. A., Lenaerts, J. T. M., Ligtenberg, S. R. M., van den Broeke, M. R., & Moholdt, G. (2013). Calving fluxes and basal melt rates of Antarctic ice shelves. *Nature*, 502(7469), 89-92.
7. Domack, E., Duran, D., Leventer, A., Ishman, S., Doane, S., McCallum, S., ... & Prentice, M. (2005). Stability of the Larsen B ice shelf on the Antarctic Peninsula during the Holocene epoch. *Nature*, 436(7051), 681-685.

8. Fretwell, P., Pritchard, H. D., Vaughan, D. G., Bamber, J. L., Barrand, N. E., Bell, R., ... & Fujita, S. (2013). Bedmap2: improved ice bed, surface and thickness datasets for Antarctica. *Cryosphere*, 7(1).
9. Frezzotti, M., Cimbelli, A., & Ferrigno, J. G. (1998). Ice-front change and iceberg behaviour along Oates and George V Coasts, Antarctica, 1912-96. *Annals of Glaciology*, 27, 643-650.
10. Holland, P. R., Corr, H. F., Pritchard, H. D., Vaughan, D. G., Arthern, R. J., Jenkins, A., & Tedesco, M. (2011). The air content of Larsen ice shelf. *Geophysical Research Letters*, 38(10).
11. Kusahara, K., Hasumi, H. & Williams, G. D. (2011), Impact of the Mertz Glacier Tongue calving on dense water formation and export. *Nature communications*, 2, 159.
12. Kwok, R. Cunningham, G. F., Zwally, H. J., & Yi, D. (2007). Ice, Cloud, and land Elevation Satellite (ICESat) over Arctic sea ice: retrieval of freeboard. *Journal of Geophysical Research*, 112, C12013, doi:10.1029/2006JC003978.
13. Legresy, B., Wendt, A., Tabacco, I. E., Remy, F., & Dietrich, R. (2004). Influence of tides and tidal current on Mertz Glacier, Antarctica. *Journal of Glaciology*, 50(170), 427-435.
14. Legresy, B., N. Young, L. Lescarmontier, R. Coleman, R.Massom, B. Giles, A. Fraser, R. Warener, B. Galton-Fenzi, L. Testut, M. Houssais and G. Masse (2010), CRAC!!! in the Mertz Glacier, Antarctica. http://www.antarctica.gov.au/__data/assets/pdf_file/0004/22549/ml_402353967939815_mertz_final_100226.pdf

15. Lescarmontier, L., Legrésy, B., Coleman, R., Perosanz, F., Mayet, C., & Testut, L. (2012). Vibrations of Mertz glacier ice tongue, East Antarctica. *Journal of Glaciology*, 58(210), 665-676.

16. Ligtenberg, S., Kuipers Munneke, P., & Van Den Broeke, M. R. (2014). Present and future variations in Antarctic firn air content. *The Cryosphere*, 8(5), 1711-1723.

17. Massom, R. A. (2003). Recent iceberg calving events in the Ninnis Glacier region, East Antarctica. *Antarctic Science*, 15(02), 303-313.

18. Massom, R. A., Giles, A. B., Fricker, H. A., Warner, R. C., Legrésy, B., Hyland, G., Young, N., & Fraser, A. D. (2010). Examining the interaction between multi-year landfast sea ice and the Mertz Glacier Tongue, East Antarctica: Another factor in ice sheet stability? *Journal of Geophysical Research*, 115, C12027, doi:10.1029/2009JC006083.

19. Massom, R. A., Giles, A. B., Warner, R. C., Fricker, H. A., Legrésy, B., Hyland, G., ... & Young, N. (2015). External influences on the Mertz Glacier Tongue (East Antarctica) in the decade leading up to its calving in 2010. *Journal of Geophysical Research: Earth Surface*, 120(3), 490-506.

20. Pavlis, N. K., Holmes S. A., Kenyon, S. C., & Factor, J. K. (2012). The development and evaluation of the Earth Gravitational Model 2008 (EGM2008), *Journal of Geophysical Research*. 117, B04406, doi:10.1029/2011JB008916.

21. Pritchard, H. D., Ligtenberg, S. R. M., Fricker, H. A., Vaughan, D. G., Van den Broeke, M. R., & Padman, L. (2012). Antarctic ice-sheet loss driven by basal melting of ice shelves. *Nature*, 484(7395), 502-505.

22. Rignot, E., Mouginot, J. & Scheuchl, B. (2011), Ice flow of the Antarctic ice sheet. *Science*, 333(6048), 1427-1430.
23. Rignot, E., & Jacobs, S. S. (2002). Rapid bottom melting widespread near Antarctic ice sheet grounding lines. *Science*, 296(5575), 2020-2023.
24. Scambos, T. Hulbe, A., C. & Fahnestock, M. A. (2003). Climate-induced ice shelf disintegration in the Antarctic Peninsula. *Antarctic Research Series,* 79, 79-92.
25. Scambos, T. Hulbe, A., C. Fahnestock, M. A. & Bohlander, J. (2000). The link between climate warming and breakup of ice shelves in the Antarctic Peninsula. *Journal of Glaciology*, 46(154), 516-530.
26. Shepherd, A., Wingham, D., Payne, T., & Skvarca, P. (2003). Larsen Ice Shelf has progressively thinned. *Science,* 302(5646), 856-859.
27. Shuman, C. A., Zwally, H. J., Schutz, B. E., Brenner, A. C., DiMarzio, J. P., Suchdeo, V. P., & Fricker, H. A. (2006). ICESat Antarctic elevation data: Preliminary precision and accuracy assessment. *Geophysical Research Letters*, 33(7).
28. Smith, K. L., Robison, B. H., Helly, J. J., Kaufmann, R. S., Ruhl, H. A., Shaw, T. J., ... & Vernet, M. (2007). Free-drifting icebergs: hot spots of chemical and biological enrichment in the Weddell Sea. *Science*, 317(5837), 478-482.
29. Smith, K. L. (2011). Free-drifting icebergs in the Southern Ocean: an overview. *Deep Sea Research Part II: Topical Studies in Oceanography*, 58(11), 1277-1284.
30. Tamura, T., Williams, G. D., Fraser, A. D. & Ohshima, K. I. (2012). Potential regime shift in decreased sea ice production after the Mertz Glacier calving, *Nature communications*, 3, 826.

31. Van den Broeke, M. (2008). Depth and density of the Antarctic firn layer. Arctic, Antarctic, and Alpine Research, 40(2), 432-438.
32. Wang, X.W., Cheng, X., Gong, P., Huang, H. B., Li Z., & Li, X. W. (2011). Earth Science Applications of ICESat/GLAS: a Review. *International Journal of Remote Sensing*, 32, 23, 8837-8864, doi: 10.1080/01431161.2010.547533
33. Wang, X.W., Cheng, X., Gong, P., Shum, C. K., Holland, D.M., & Li, X.W. (2014). Freeboard and mass extraction of the disintegrated Mertz Ice Tongue with remote sensing and altimetry data. *Remote Sensing of Environment*, 144, 1-10.
34. Wang, X.W. (2014). Mertz ice tongue evolutions from satellite observed data, Postdoctoral Research Report, College of Global Change and Earth System Science, Beijing Normal University, China. doi: 10.13140/2.1.1006.1603
35. Wang, X., Cheng, X., Li, Z., Huang, H., Niu, Z., Li, X., & Gong, P. (2012). Lake water footprint identification from time-series ICESat/GLAS data. *IEEE Geoscience and Remote Sensing Letters*, 9(3), 333-337.
36. Wang, X., Gong, P., Zhao, Y., Xu, Y., Cheng, X., Niu, Z., ... & Li, X. (2013). Water-level changes in China's large lakes determined from ICESat/GLAS data. *Remote Sensing of Environment*, 132, 131-144.
37. Yi, D., Zwally, H.J., & Robbins, J. (2011). ICESat observations of seasonal and interannual variations of sea-ice freeboard and estimated thickness in the Weddell Sea, Antarctica (2003-2009). *Annals of Glaciology*, 52(57), 43-51.
38. Zwally, H. J., Schutz, B., Abdalati, W., Abshire, J., Bentley, C., Brenner, A., Buftona, J., Deziof, J., Hancocka, D., Hardinga, D., Herringg, T., Minsterh, B., Quinng, K., Palmi,

646 S., Spinhirnea, J., & Thomasj, R. (2002). ICESat's laser measurements of polar ice,
647 atmosphere, ocean, and land. *Journal of Geodynamics*, 34, 405-445.
648 39. Zwally, H. J., Yi, D., Kwok, R., & Zhao, Y. (2008). ICESat measurements of sea ice
649 freeboard and estimates of sea ice thickness in the Weddell Sea. *Journal of Geophysical*
650 *Research*, 113, C02S15, doi:10.1029/2007JC004284.
651

Figures

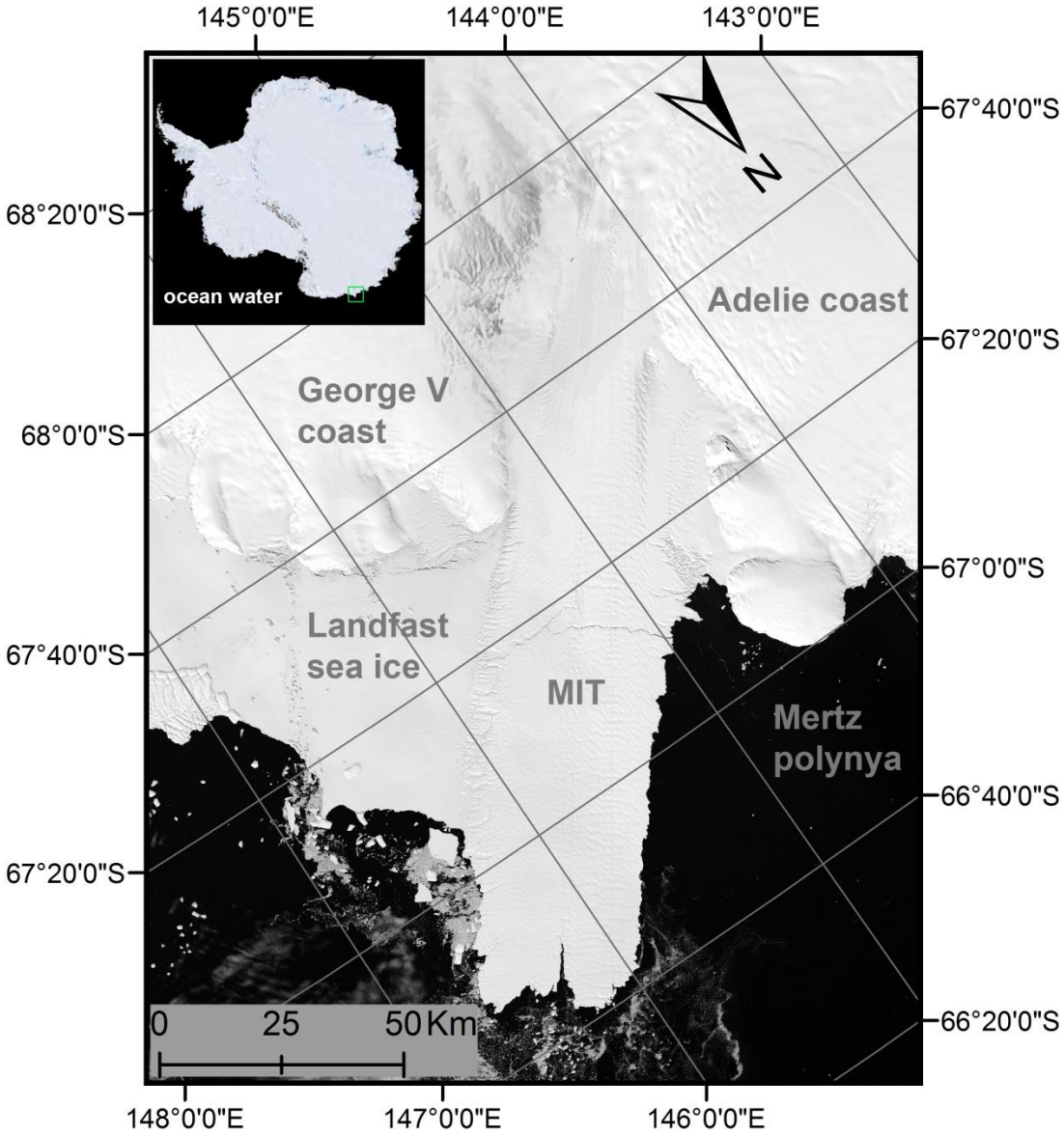

Figure 1. Mertz Ice Tongue (MIT), East Antarctica. Landfast sea ice is attached to the east flank of the MIT and the Mertz Polynya is to the west. The background image corresponds to band 4 Landsat 7, captured on February 2, 2003. The green square found in the upper left inset indicates the location of the MIT in the East Antarctica. A polar stereographic projection with -71 ºS as standard latitude is used.

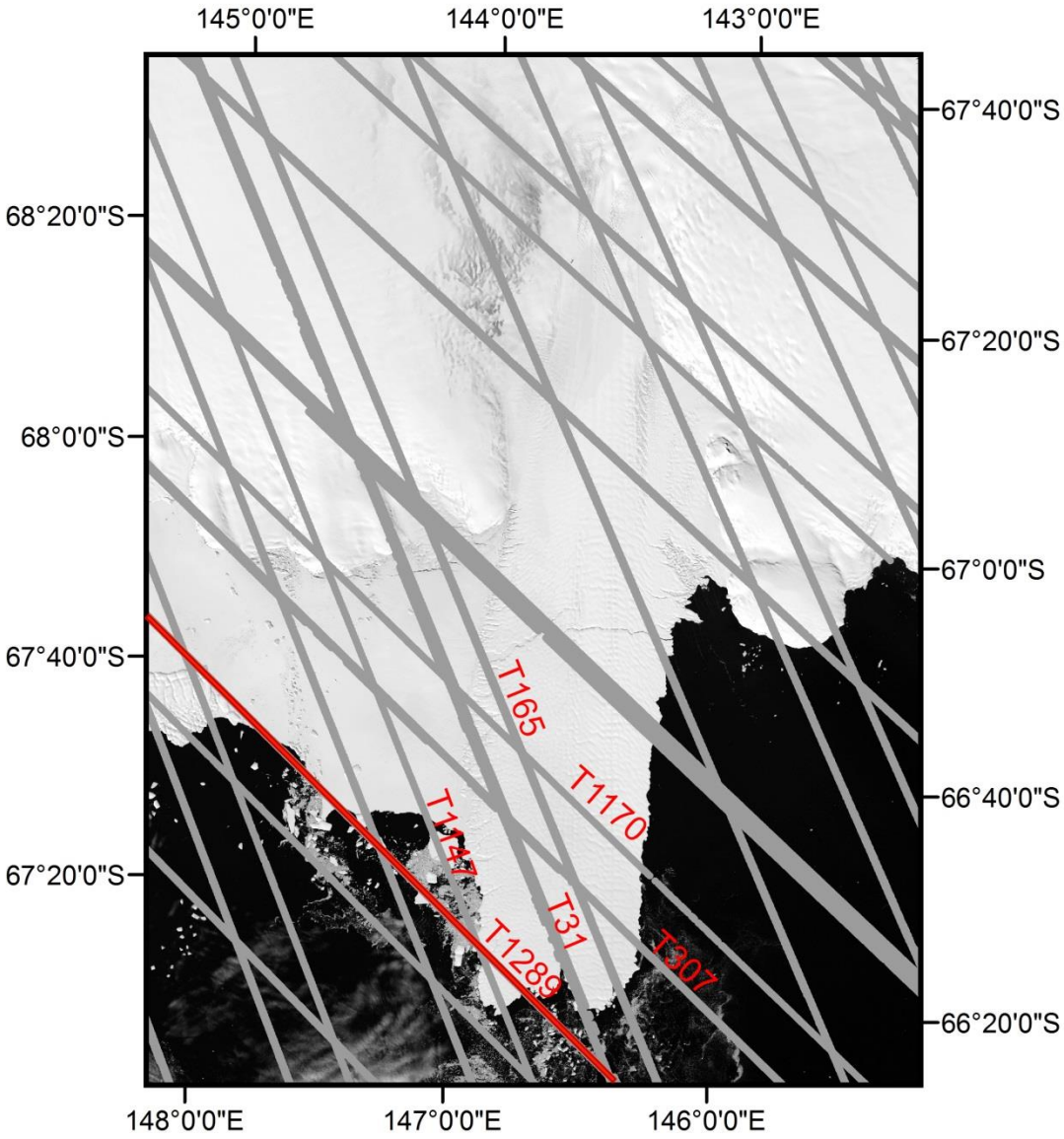

Figure 2. Spatial distribution of the ICESat/GLAS data from 2003 to 2009 covering the Mertz region. Ground tracks of ICESat/GLAS are indicated with gray lines. Track 1289 (T1289) is highlighted in red as is used in Fig. 4. The background image corresponds to band 4 Landsat 7, captured on February 2, 2003. A polar stereographic projection with -71 ℃S as standard latitude is used.

666

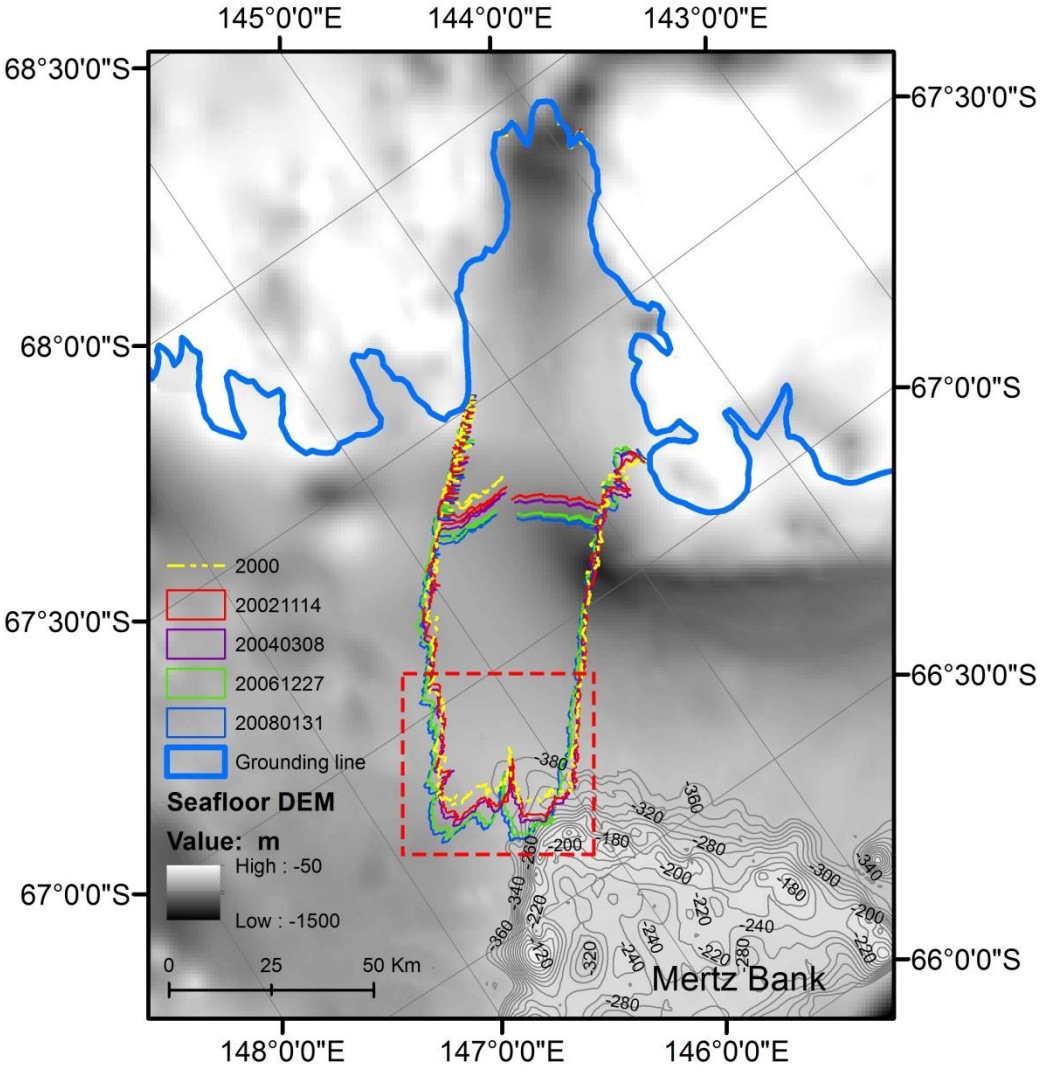

667

668 (a)

669

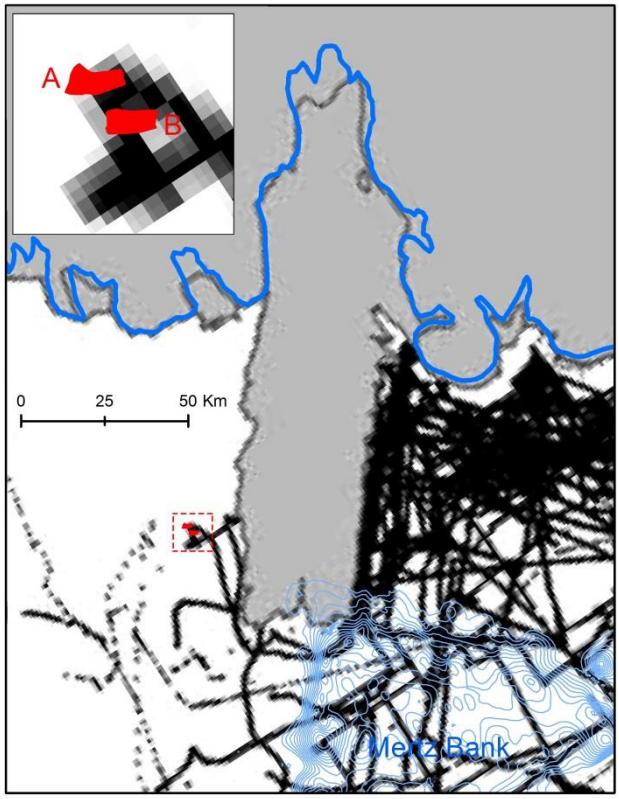

(b)

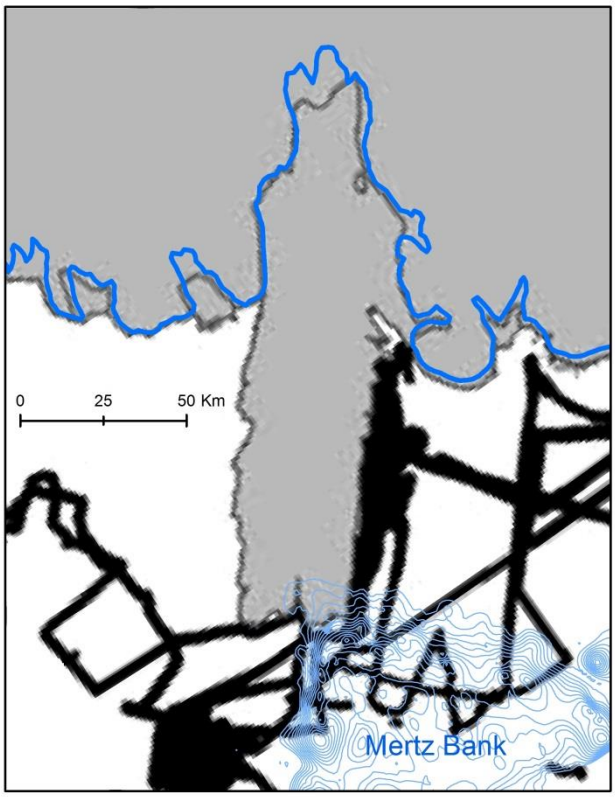

(c)

Figure 3. (a) Seafloor topography from bathymetry around Mertz and the outlines of the MIT from 2002 to 2008 marked with the colored polygons for different years. The shallow Mertz Bank is located in the lower right (northeast). The yellow dash-dotted line indicates the shape of the MIT from January 25, 2000, which is used to identify the bathymetry gap under the ice tongue. The dashed red inset box corresponds to the location of Figs. 6 and 7. (b) : multi-beam bathymetry dataset coverage over the Mertz region. The embedded figure in the upper left is the zoom in of the dashed red rectangle which shows the positions of icebergs 'A' and 'B' (polygon filled in red) on February 19, 2008 (Fig. 4b). (c): single-beam bathymetry dataset coverage over the Mertz region. The light blue polylines show the contours around the Mertz Bank and the black dots are bathymetric measurement profiles. Both (b) and (c) are redrawn from Beaman et

686 al. (2011) because the original spatial coverage of the single and multi-beam bathymetry data is
687 not available. However, for being able to use the Figures from Beaman et al. (2011), we geo-
688 registered it and put the contour around the Mertz Bank and the location of icebergs used in the
689 text over it, from which the density of the bathymetry measurements can be clear. Through
690 comparing the grounding lines from (b) and (c), we can conclude that the geo-registration is
691 successful as the grounding line we obtained from the National Snow and Ice Data Center
692 (NSIDC) coincides with that from Beaman et al. (2011) well in most parts. This Figure is under a
693 projection of polar stereographic projection with -71 ℃S as standard latitude.

694

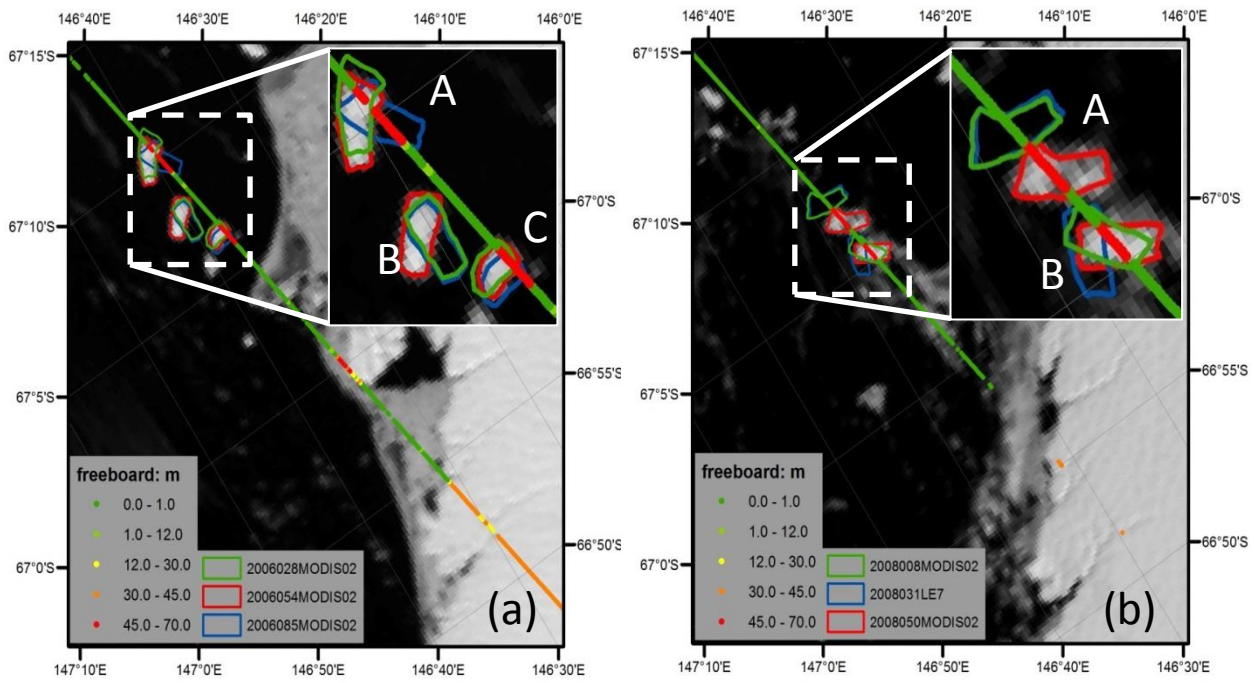

695

696 **Figure 4.** Freeboard extracted from Track T1289, ICESat/GLAS, the location of which can be
697 found from Fig. 2 and Fig. 3(b). (a) and (b) show the freeboard extracted from the ICESat/GLAS
698 date from February 23, 2006 (2006054) and February 18, 2008 (2008049) respectively. In each
699 image, the positions of three icebergs (with name labeled as 'A', 'B' and 'C') closest to the
700 ICESat/GLAS observation date are plotted with green, red and blue polygons respectively. The
701 observation dates of remote sensing images are indicated with seven numbers (yyyyddd) in the
702 legend. 'yyyyddd' stands for day 'ddd' in year 'yyyy'. 'MODIS02' and 'LE7' indicate that the
703 images used to extract outlines of the icebergs are from MODIS and Landsat 7 ETM+,
704 respectively.

705

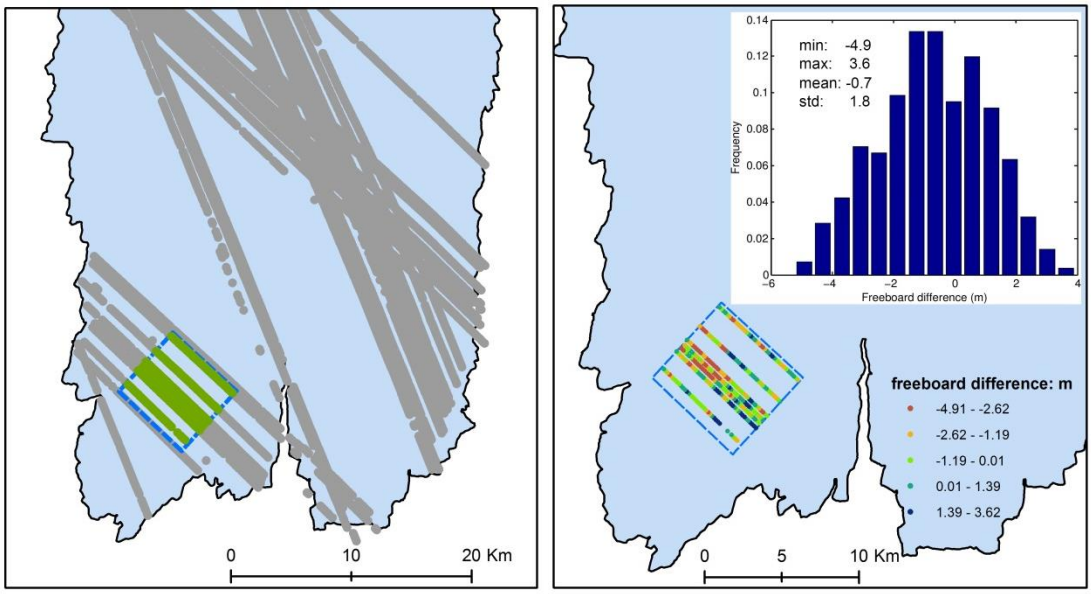

(a) (b)

Figure 5. Evaluation of kriging interpolation method over the MIT using freeboard data derived from the ICESat/GLAS data. (a) shows profile location of freeboard derived from the ICESat/GLAS data after relocation over the MIT. The gray dots indicate the ICESat/GLAS data used for interpolation using kriging method. The blue dashed square indicates the region used to investigate the accuracy of kriging interpolation method, 7 km×7 km in size. Inside the square, the freeboard data marked with green dots are used to check the accuracy of the freeboard interpolated with kriging. (b) is the freeboard comparison result derived by subtracting the krigged freeboard from the freeboard derived from the ICESat/GLAS. The spatial distribution and the histogram of the freeboard difference are shown in the lower left and upper right respectively. The black polygon filled with light blue shows the boundary of the MIT on November 14, 2002.

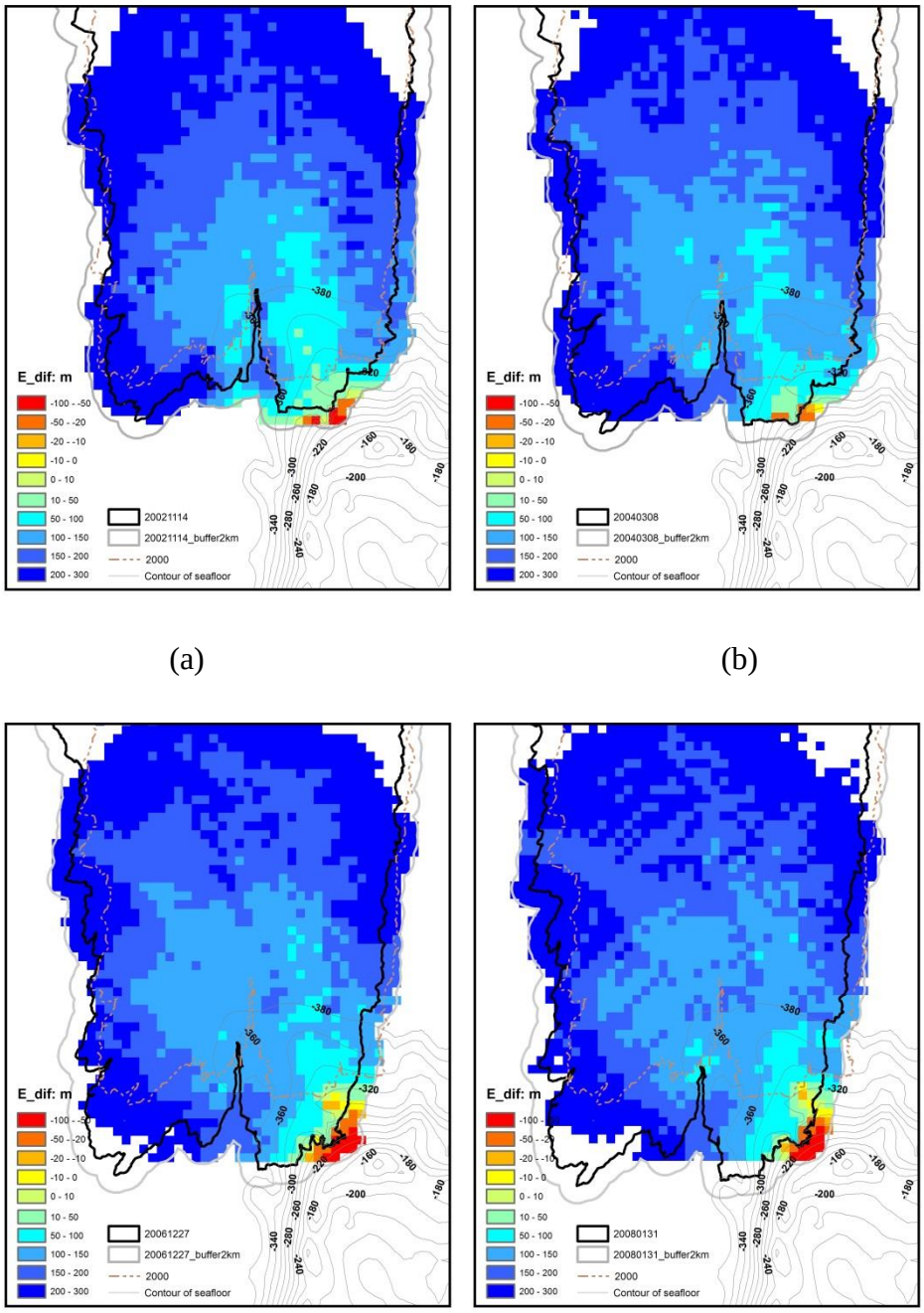

721

722 (a) (b)

723

724 (c) (d)

725 **Figure 6.** Elevation difference of Mertz ice bottom and seafloor topography. (a), (b), (c) and (d)

726 correspond to the elevation difference from November 14, 2002 , March 8, 2004, December 27,

727 2006, and January 31, 2008, respectively assuming hydrostatic equilibrium under the minimum

728 sea surface height -3.35 m . The contours at an interval of 20 m in the lower right indicate the

729 seafloor topography of the Mertz Bank. The solid black line indicates the boundary of the MIT
730 and the thick gray line outlines a buffer region of the boundary with 2 km as buffer radius. The
731 dash-dotted line indicates the shape of the MIT on January 25, 2000, which is used to identify
732 the bathymetry gap under the MIT. In the legend, the negative values mean that the ice bottom is
733 lower than the seafloor, which of course is impossible. Therefore, the initial assumption of a
734 floating ice tongue was incorrect in those locations (yellow to red colors), and the ice was
735 grounded. Regions with more negative values indicate heavier grounding inside the MIT or
736 grounding potential in the buffer region. Please note that no bathymetric data was available
737 under most of the ice tongue and for locations of the bathymetric data, please refer to Figs 3b and
738 3c.

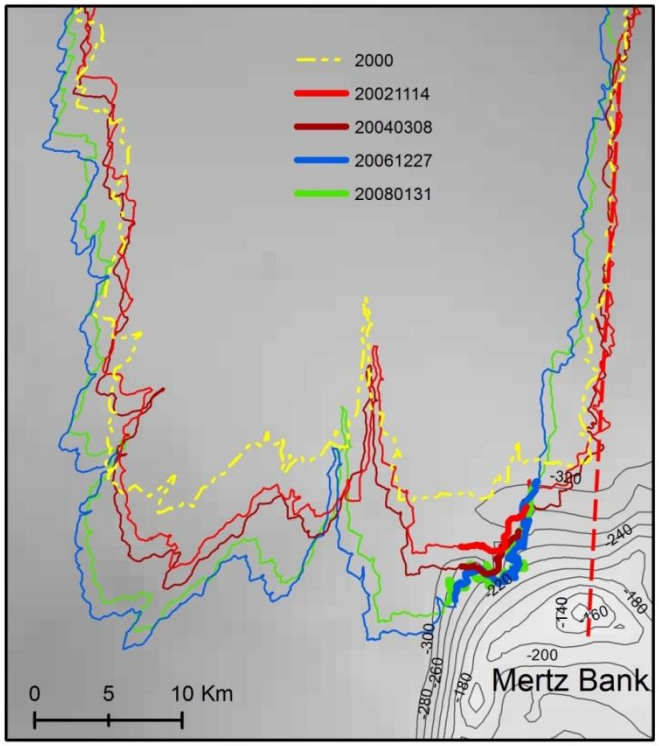

739

740 **Figure 7**. Digital Elevation Map (DEM) of seafloor around the Mertz and grounding section of
741 the boundaries extracted from 2002 to 2008. The grounding sections of the MIT boundary from
742 2002, 2004, 2006 and 2008 are marked with thick red, purple, green and blue polylines
743 respectively and the MIT boundaries are indicated with polygons with the same legend as that in
744 Fig. 3a. Additionally, the MIT boundary from 2000 indicated with dash-dotted yellow polygon
745 is used to show the different quality of the seafloor DEM. Inside this polygon no bathymetry data
746 was collected or used. The dashed red line indicates the 'extension line' of the west flank of the
747 MIT on November 14, 2002, passing the shallowest region of the Mertz Bank (approximately -
748 140 m).

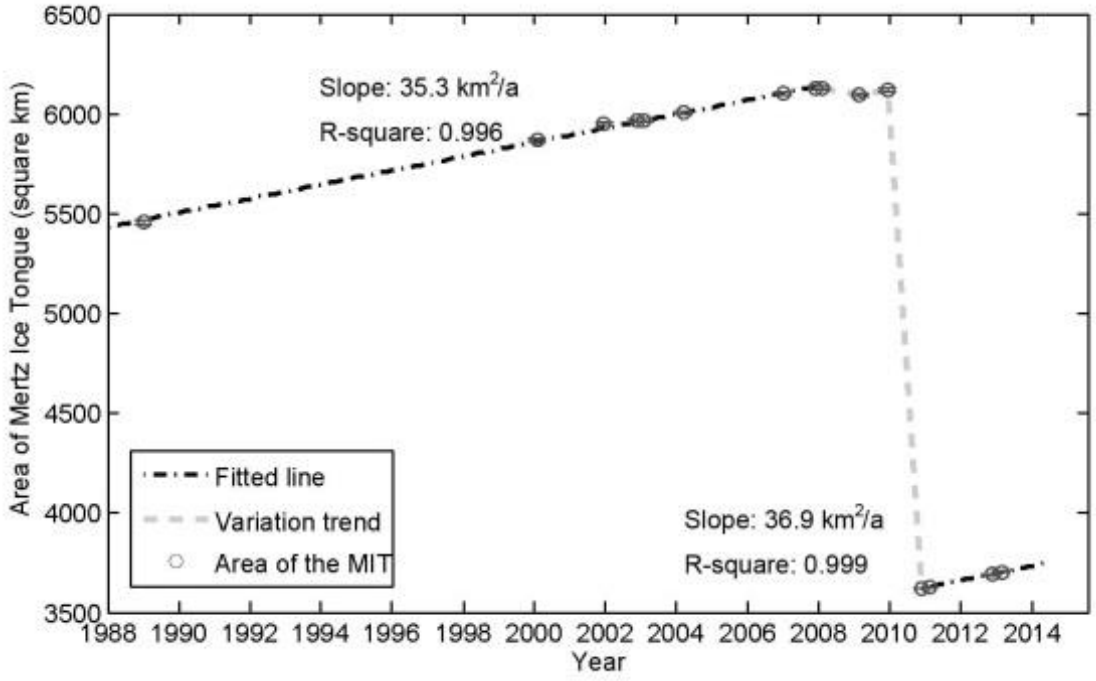

749

750 **Figure 8**. Average trend of the area change of the MIT. The area of the MIT is extracted from

751 the Landsat images from 1988 to 2013.

752

Tables

Table 1. Statistics of icebergs used to invert FAC with a least-square method and validation of grounding iceberg detection using this FAC. Icebergs 'A', 'B' and 'C' are the same as what are used in Fig. 4 and S-Fig 1. The measurements from icebergs 'A' and 'C' in February, 2006 are used to derive the FAC with a least-squares method. However, the measurements from Icebergs 'A' and 'B' in 2008 are used for validation.

Icebergs	date	Latitude (°)	Longitude (°)	Freeboard (m)	Seafloor (m)	Sea Surface Height (m)	ε (m)	E_{dif} (m)
A	Feb 23, 2006	-67.1737	146.6595	66.88	-528.48	-1.92	0.89	
		-67.1752	146.6604	66.34	-527.01	-1.92	1.30	
C	Feb 23, 2006	-67.1085	146.6247	66.37	-505.84	-1.92	-1.25	
		-67.1100	146.6255	66.28	-507.08	-1.92	-1.01	
A	Feb 18, 2008	-67.1194	146.6303	58.88	-522.52	-2.08		69.14
		-67.1209	146.6311	59.58	-524.16	-2.08		64.88
B	Feb 18, 2008	-67.0906	146.6151	67.22	-500.92	-2.08		-22.45
		-67.0921	146.6159	66.10	-500.47	-2.08		-13.55

760 **Table 2**. Statistics of grounding grids inside the MIT or grounding potentials outside of the MIT
761 ('I': inside the thick black line, Fig. 6; Number in brackets indicates how many grids are located
762 inside the 2000 Mertz boundary; 'O': between the black and gray lines, Fig. 6) from November
763 14, 2002, March 8, 2004, December 27, 2006 and January 31, 2008 respectively. Each grid
764 covers an area of 1 km^2. The Mean, Minimum and Standard deviation is calculated without
765 considering those fallen inside the 2000 Mertz boundary, but only those out of 2000 Mertz
766 boundary with elevation difference less than 46 m.

767

Elevation difference (subtracting seafloor from ice bottom)	2002-11-14		2004-03-08		2006-12-27		2008-01-31	
	I	O	I	O	I	O	I	O
23-46 (m)	9(3)	10(0)	6(0)	3(0)	10(1)	1(0)	10(3)	5(0)
0-23 (m)	2(0)	6(0)	1(0)	1(0)	9(0)	2(0)	4(0)	2(0)
<0 (m)	0(0)	8(0)	2(0)	5(0)	7(0)	21(0)	6(0)	18(0)
Mean (m)	28.8	9.8	15.8	-1.1	10.9	-41.9	12.3	-31.0
Minimum (m)	11.9	-81.5	-46.0	-44.5	-52.3	-102.8	-34.8	-103.0
Standard deviation (m)	9.2	36.8	29.6	31.4	24.7	37.6	27.3	38.0
Number of grids	8	24	9	9	25	24	17	25

768

769 **Table 3**. Statistics of grounding outlines of the MIT as shown with thick polylines in Fig. 7 from

770 November 14, 2002, March 8, 2004, December 27, 2006 and January 31, 2008 respectively

	2002-11-14	2004-03-08	2006-12-27	2008-01-31
Start location (°)	146.124 °E, 66.696 °S	146.155 °E, 66.681 °S	146.093 °E, 66.700 °S	146.088 °E, 66.699 °S
End location (°)	146.240 °E, 66.693 °S	146.256 °E, 66.683 °S	146.304 °E, 66.669 °S	146.292 °E, 66.668 °S
Perimeter (km)	7.0	6.4	24.7	20.9

771